

Conformational Selection of a Tryptophan Side Chain Drives the Generalized Increase in Activity of PET Hydrolases through a Ser/Ile Double Mutation

Alessandro Crnjar,¹ Aransa Griñen,¹ Shina C. L. Kamerlin,* and César A. Ramírez-Sarmiento*



Cite This: *ACS Org. Inorg. Au* 2023, 3, 109–119



Read Online

ACCESS |

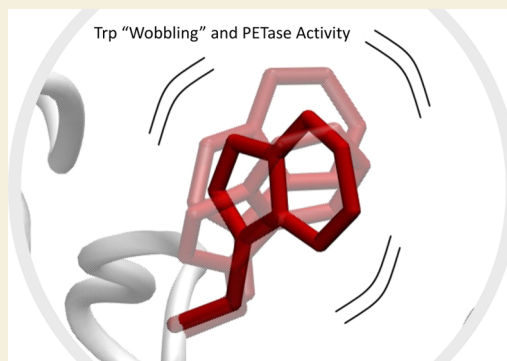
Metrics & More

Article Recommendations

Supporting Information

ABSTRACT: Poly(ethylene terephthalate) (PET) is the most common polyester plastic in the packaging industry and a major source of environmental pollution due to its single use. Several enzymes, termed PET hydrolases, have been found to hydrolyze this polymer at different temperatures, with the enzyme from *Ideonella sakaiensis* (*IsPETase*) having optimal catalytic activity at 30–35 °C. Crystal structures of *IsPETase* have revealed that the side chain of a conserved tryptophan residue within an active site loop (W185) shifts between three conformations to enable substrate binding and product release. This is facilitated by two residues unique to *IsPETase*, S214 and I218. When these residues are inserted into other PET hydrolases in place of the otherwise strictly conserved histidine and phenylalanine residues found at their respective positions, they enhance activity and decrease T_{opt} . Herein, we combine molecular dynamics and well-tempered metadynamics simulations to investigate dynamic changes of the S214/I218 and H214/F218 variants of *IsPETase*, as well as three other mesophilic and thermophilic PET hydrolases, at their respective temperature and pH optima. Our simulations show that the S214/I218 insertion both increases the flexibility of active site loop regions harboring key catalytic residues and the conserved tryptophan and expands the conformational plasticity of this tryptophan side chain, enabling the conformational transitions that allow for substrate binding and product release in *IsPETase*. The observed catalytic enhancement caused by this substitution in other PET hydrolases appears to be due to conformational selection, by capturing the conformational ensemble observed in *IsPETase*.

KEYWORDS: PET hydrolases, plastic recycling, molecular dynamics, metadynamics, enzyme design



INTRODUCTION

The inexpensive manufacturing, long-term durability, and high resistance to degradation of plastics have led to its concerning accumulation as waste in landfills and oceans at rates that parallel its annual production.¹ The primary sources of plastic waste are single-use or short-lifetime consumer plastics, mainly poly(ethylene terephthalate) (PET), polyethylene (PE), and polypropylene (PP), with PET being the predominant polymer in postconsumer domestic plastic waste collected in countries such as the UK (40% abundance).²

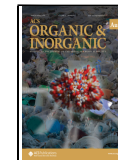
Although PET is recognized as one of the most recyclable plastics due to the vast presence of mechanical recycling industries, it can only endure a limited number of cycles before its properties are compromised. For example, the tensile and impact strength of virgin PET used in bottles decreases almost linearly within the first three extrusion cycles,³ whereas its ductility is reduced from >200 to <10% elongation at break upon mechanical recycling.⁴ Consequently, recycled PET ends up being used in lower-grade PET applications that are seldom recycled, breaking the circularity of this process.

In this context, the discovery of PET hydrolases^{5,6} has emerged as a promising and environmentally friendly approach

for plastic biorecycling.^{7,8} These enzymes depolymerize PET into its main constituent monomers, which can then be used to resynthesize virgin PET and thus enable a fully circular plastic recycling process.⁹ Most PET hydrolytic enzymes are thermophilic,⁵ with optimal activities (~65 °C) near the glass-transition temperature of PET (~75 °C¹⁰), where the polymer chains become more flexible and are prone to enzymatic hydrolysis, due to the inability of PET hydrolases to degrade highly crystalline PET. However, a PET hydrolase from the mesophilic bacterium *Ideonella sakaiensis* 201-F6 (*IsPETase*) was described to degrade amorphous and semi-crystalline PET with high efficiency at 30–35 °C.¹¹

While most known PET hydrolytic enzymes have been subjected to protein engineering via rational design or directed

Received: October 7, 2022
Revised: December 15, 2022
Accepted: December 15, 2022
Published: January 9, 2023



evolution, with substantial improvements in thermal stability and depolymerase activity,¹² finding a “one size fits all” solution to improve the catalytic efficiency of any PET hydrolase has been elusive. A recent work¹³ presented a general mechanism for improving their catalytic activity based on the experimentally observed dihedral torsions of a conformationally dynamic tryptophan side chain in *IsPETase*, W185 (Figure 1), that is highly conserved in PET hydrolases in

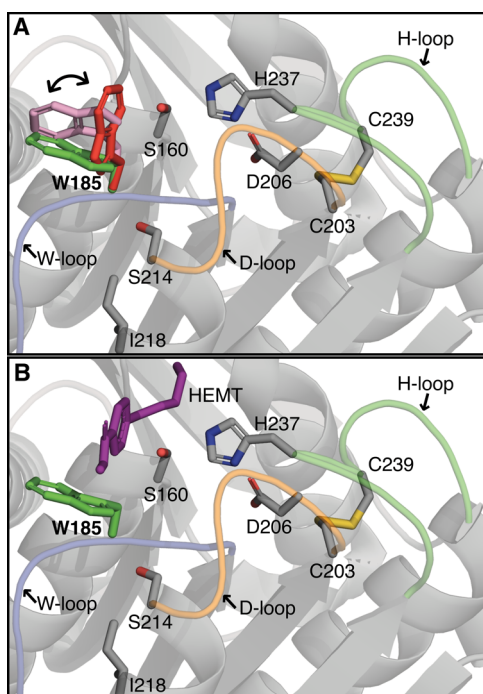


Figure 1. Multiple conformations of W185 observed in crystal structures of free and substrate-bound *IsPETase*. Cartoon representation of the active site of *IsPETase* (A) in the absence (PDB ID: 5XG0¹⁴) and (B) in the presence of the substrate analogue HEMT (PDB ID: 5XH3¹⁴). The key catalytic residues (S160, D206, H237), the active site disulfide bond (C203-C239), the W185 side chain, and the critical S214/I218 residues are shown in sticks. The different conformers of W185 are shown in red (conformer A), green (conformer B), and pink (conformer C). Relevant loops harboring W185 (W-loop), D206 (D-loop), and H237 (H-loop) are colored blue, orange, and green, respectively. The substrate analogue 1-(2-hydroxyethyl) 4-methyl terephthalate (HEMT) forms a T-shaped interaction with W185. Loops in cartoon representation were smoothed for visualization purposes.

a loop within the active site (hereafter referred to as the W-loop). On a nearby helix, there are two residues, S214 and I218, which are unique to *IsPETase*, and in all other known PET hydrolytic enzymes correspond to histidine and phenylalanine.

Crystal structures of *IsPETase* in the absence of substrates (PDB ID: 5XG0¹⁴) show that the W185 side chain can adopt three conformations, termed A, B, and C, as illustrated in Figure 1, a phenomenon that has been described in the literature as “wobbling”.¹⁵ Substrate analogue-bound enzyme complexes (PDB IDs: 5XH2¹⁴ and 5XH3¹⁴) show that this residue adopts conformer B for substrate binding, where it can form T-shaped, stacked, or parallel displaced interactions with one of the terephthalic rings of the substrate. Comparison of the crystal structure of *IsPETase* against a thermophilic PET hydrolase from a leaf-branch compost metagenome (LCC)

suggests that the small size of S214 yields sufficient space for W185 to rotate to accommodate the substrate.¹⁵ Altogether, it is thought that tryptophan motion is relevant for substrate binding and product release. Consistently with this, the S214H mutant of *IsPETase* shows decreased activity compared to the wild-type enzyme.¹⁴

We note that there have been multiple elegant computational studies that have helped reveal the mechanisms of PET-degrading enzymes,^{16–19} more global conformational changes involved in catalysis,^{20,21} and contributed to associated engineering effort.^{22–25} However, corresponding studies of the conformational dynamics of this catalytically important tryptophan remain limited. Therefore, to explore the importance of the S214/I218 substitution for PET hydrolytic activity, doubly substituted variants of the strictly conserved histidine and phenylalanine residues in several PET hydrolases, including the mesophilic *BurPL* from a *Burkholderiales* bacterium (H344/F348),¹³ and the thermophilic *TfCut* from *Thermobifida fusca* (H224/F228)²⁶ and LCC (H218/F222),²⁷ were generated based on the S214/I218 residues unique to *IsPETase*. All engineered variants have experimentally shown an increase in PET-degrading activity.¹³ Conversely, an H214/F218 variant of *IsPETase* exhibits a decrease in PET hydrolase activity.¹³ The enhancement in PET hydrolysis caused by the S214/I218 substitution is accompanied by a decrease in the optimal temperature for catalytic activity (T_{opt}), suggesting that the substitutions impact either the local or global stability of these enzymes.

In this work, we employ molecular dynamics (MD) and well-tempered metadynamics²⁸ simulations to explore the structural basis of the improved catalytic activity of *BurPL*, *TfCut*, and LCC upon incorporation of the *IsPETase*-based S214/I218 double substitution. Our results show that these substitutions increase the flexibility of both active site loop regions harboring key catalytic residues, and the conformational plasticity of the conserved tryptophan within the W-loop. Notably, while all of the experimentally determined tryptophan conformers are accessible for all enzymes, the *IsPETase*-based S214/I218 substitution appears to facilitate population shifts to and from conformer A, as well as other conformations, such as a 180° side chain rotation that has not been observed in any solved crystal structures of PET hydrolases. Overall, our simulations provide evidence for a dynamical origin for the enhanced catalytic activity of the doubly substituted variants, affecting both loop dynamics and the conformational plasticity of the tryptophan.

METHODOLOGY

Preparation of Initial Structures

Initial coordinates for wild-type *BurPL* (H344/F348), LCC (H218/F222), and *TfCut* (H224/F228) were obtained from the crystal structures deposited in the Protein Data Bank²⁹ under PDB IDs: 7CWQ,¹³ 4EB0,²⁷ and 5ZOA,³⁰ respectively. For *IsPETase*, the initial structure corresponded to the recently solved structure of the single-point mutant S214H, PDB ID: 7CY0,¹³ where the serine residue in S214/I218 was replaced by the histidine that is strictly conserved in other PET hydrolytic enzymes. The doubly substituted versions of *BurPL* (S344/I348), *TfCut* (S224/I228), and LCC (S218/I222), as well as the S214/I218 and H214/F218 variants of *IsPETase*, were generated using the Mutagenesis tool in PyMOL v. 2.4.2.³¹

Both *IsPETase* and *BurPL* harbor an active site (C203-C239 for *IsPETase*, C333-C370 for *BurPL*) and a C-terminal (C273-C289 for *IsPETase*, C404-C424 for *BurPL*) disulfide bond. For *TfCut* and *LCC*, only the C-terminal disulfide bond (C281-C299 for *TfCut*, C275-C292 for *LCC*) is present. These disulfide bonds, which are present in the available crystal structures, were kept in all of the wild-type enzymes and doubly substituted variants.

Residue numbers for each enzyme are presented throughout the main text according to the full-length amino acid sequences of these proteins in the Uniprot database,³² with accession IDs: A0A0K8P6T7 (*IsPETase*), A0A1F4JXW8 (*BurPL*), Q6A0I4 (*TfCut*), and G9BY57 (*LCC*).

Molecular Dynamics Simulations

MD simulations were performed using the pmemd.cuda implementation of the AMBER 2020 simulation package,³³ along with the ff14SB force field³⁴ and the TIP3P³⁵ water model for the parameters of protein atoms and water molecules, respectively. For each of the eight simulation systems, the protonation state of each residue at pH 9.0 was estimated with the H++ server,³⁶ to match the experimental conditions in enzymatic degradation assays using either PET films or granules.¹³ The consistency of the estimated protonation states for the wild-type and doubly substituted variant of each enzyme was manually checked. The residues affected by the choice of pH include the catalytic histidine in all four enzymes (which would be protonated at pH 7), alongside E334 and H408 in *BurPL*, which are not part of the active site cleft. The $pK_{1/2}$ of these residues, employed by the H++ server to compute whether they should be protonated or not depending on the pH, is reported in Table S1. Then, all systems were solvated in truncated octahedral water boxes with 15 Å of padding and neutralized with Na⁺ or Cl⁻ counterions. A standard minimization, heating, and 10 ns equilibration protocol were performed, followed by NPT production at 1 bar and the experimentally determined optimal temperature of catalytic activity for each system¹³ (i.e. 303 K for *IsPETase*, 308 K for *BurPL*, 323 K for *LCC*, and 333 K for *TfCut*). Constant temperature and pressure conditions for each system were controlled using a Langevin thermostat³⁷ with a collision frequency of 1 ps⁻¹, and a Berendsen barostat³⁸ with a pressure relaxation time of 1 ps. MD simulations were run using a time step of 2 fs along with the SHAKE³⁹ algorithm to constrain hydrogen-containing bonds, a 12 Å cutoff for nonbonded interactions, and the particle-mesh Ewald⁴⁰ method for long-range electrostatics. Five 500 ns long replicas were produced for each of the wild-type and doubly substituted systems, for a total of 20 μs of MD simulations. The convergence of the simulations is shown in Figure S1.

Well-Tempered Metadynamics Simulations

To study the torsional free energy associated with rotation of the conserved W-loop tryptophan, we performed eight 400-ns-long well-tempered metadynamics²⁸ simulations (one per system), using the AMBER 2020³³ simulation package and Plumed 2.7.⁴¹ We used as collective variables (CVs) the χ_1 (N-C_α-C_β-C_γ) and χ_2 (C_α-C_β-C_γ-C_{δ2}) dihedral angles, which describe the torsional space of the tryptophan side chain. Metadynamics runs were started after 50 ns of NPT equilibration (following the same protocol and simulation settings as the MD). The backbone root-mean-square deviation (RMSD) of the helices and β-sheets of the protein structure, and the convergence of our metadynamics runs, are

shown in Figures S2–S4. Simulations were performed using a bias factor of 12, a Gaussian width of 9° per CV, a Gaussian initial height of 0.1 kcal/mol, and a deposition rate of 1 ps⁻¹. The convergence of these simulations was checked by monitoring the evolution of the CVs over time together with the free energy profile.

The free energy surface as a function of the two chosen CVs was calculated according to the theory of well-tempered metadynamics.^{28,42} Given the deposited bias potential, V

$$V(\chi_1, \chi_2, t) = \sum W \exp \left(\frac{-(\chi_1 - \chi_1(n\tau))^2}{2\sigma_{\chi_1}^2} \right. \\ \left. - \frac{(\chi_2 - \chi_2(n\tau))^2}{2\sigma_{\chi_2}^2} \right) \quad (1)$$

where χ_1 and χ_2 denote the two selected CVs, τ denotes the time step, n denotes the number of steps until time t (so that the sum runs over all steps $n\tau < t$), and σ_{χ_1} and σ_{χ_2} denote the Gaussian widths associated with the two CVs. In well-tempered metadynamics, W is also a function of time such that

$$W(t) = W_0 e^{-V(\chi_1, \chi_2, t)/k_B \Delta T} \quad (2)$$

Here, W_0 is the initial height and ΔT is a parameter linked to the bias factor, γ , by the following equation

$$\gamma = (T + \Delta T)/T \quad (3)$$

Over long simulation timescales, this bias potential converges to the free energy, F

$$V(\chi_1, \chi_2, t \rightarrow \infty) = \frac{-\Delta T}{T + \Delta T} F(\chi_1, \chi_2) + C \quad (4)$$

with C being a constant that, for well-tempered metadynamics, vanishes for a long enough time (i.e., once the diffusive state in the collective variable space has been reached). Finally, the free energy was evaluated as a function of the CVs using the Tiwary method⁴³

$$\beta F(\chi_1, \chi_2) = \frac{-\gamma V(\chi_1, \chi_2, t)}{k_B \Delta T} \\ + \log \int d\chi_1 d\chi_2 e^{\gamma V(\chi_1, \chi_2, t)/k_B \Delta T} \quad (5)$$

Simulation Analysis

Simulation analysis was performed using the CPPTRAJ⁴⁴ module from AMBER 2020³³ and the Python library MDAnalysis.^{45,46} Snapshots were collected every 50 ps from the MD production runs for further analysis. Open cleft volume analysis was performed using POCKET Volume MEasurer (POVME) 3.0,⁴⁷ by considering 1000 frames over all replicas, taken every 2.5 ns of the production run. An initial sphere of radius 4 Å located at the center of mass between the α-carbon atoms of residues Y87 and M161 (*IsPETase*), Y217 and M291 (*BurPL*), Y100 and S170 (*TfCut*), and Y95 and S165 (*LCC*) was used for the calculations. The residues forming the cleft are represented in Figure S5 and listed in Table S2. Root-mean-square fluctuations (RMSF) were calculated on the C_α atoms along the amino acid sequence of each protein relative to their averaged position over time. Hydrogen bonds for catalytic residues were calculated by considering a donor–acceptor distance cutoff of 3.5 Å and a donor–hydrogen–acceptor angle cutoff of 120°, considering

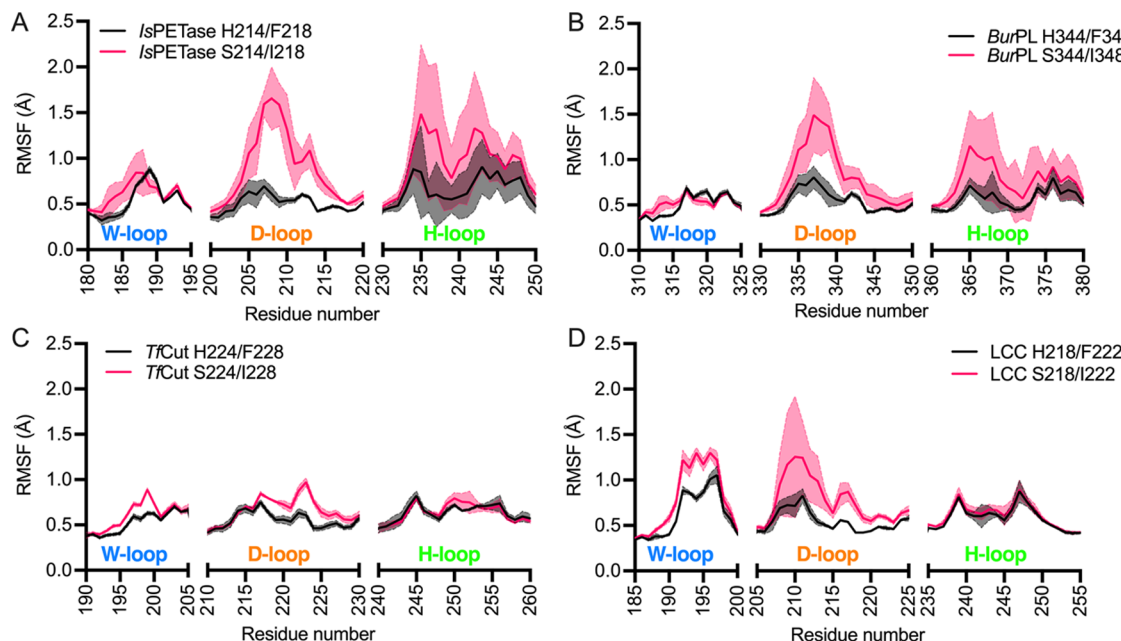


Figure 2. Effect of the *IsPETase*-based S214/I218 substitution on the local structural flexibility of PET hydrolases. (A–D) C_α atom root-mean-square fluctuations (RMSF, Å) of the flexible active site W-loop, D-loop, and H-loop (shown in Figure 1) during MD simulations of the *IsPETase*-based S214/I218 (pink) and H214/F218 (black) variants of (A) *IsPETase*, (B) *BurPL*, (C) *TfCut*, and (D) *LCC*. The shaded area represents the standard deviation over 5×500 ns trajectories per system.

all 25,000 frames collected per replica. The same number of frames was employed for calculating the change in distance between the C_γ atoms of the conserved tryptophan in the W-loop and the conserved tyrosine with which it forms an active site aromatic clamp.²⁰ Finally, shortest path map (SPM) analysis was carried out by means of the *DynaComPy* Python script,⁴⁸ using the dynamic cross-correlation matrices and average inter-residue distance matrices for the MD simulations.

RESULTS AND DISCUSSION

To determine the effects of the S214/I218 double substitution on PET hydrolase dynamics, we analyzed the root-mean-square fluctuations (RMSF) of the H214/F218 and S214/I218 variants of *IsPETase* and of the equivalent variants for *BurPL*, *TfCut*, and *LCC* across a cumulative $2.5 \mu\text{s}$ of conventional MD simulations of each unliganded system (5×500 ns trajectories per system) at their respective temperature and pH optima. In all cases, comparison of the variants for each enzyme did not show significant differences in RMSF throughout the protein (Figure S6), except for the W- and D-loops (Figure 2), which harbor the conserved active site tryptophan (W185 in *IsPETase*) and the catalytic aspartic acid (D206 in *IsPETase*), respectively.

From the data shown in Figure 2, it is observed that in *IsPETase*, the substitution of S214/I218 by H214/F218 reduces the flexibility of the D-loop. Conversely, in the other PET-degrading enzymes, which harbor histidine and phenylalanine in their wild-type forms, the double substitution by serine and isoleucine increases the overall flexibility of the D-loop and, in the case of *TfCut* and *LCC*, the W-loop (although the precise magnitude of this effect varies by enzyme and specific loop). Moreover, the H-loop is more flexible in the serine and isoleucine variants of *IsPETase* and *BurPL* than in *TfCut* and *LCC*, despite harboring the active site disulfide bond connecting the D-loop and H-loop in the mesophilic enzymes (Figure 1). This could be explained by the longer

extension of the H-loop in *IsPETase* and *BurPL* than in the thermophilic enzymes, which enables the formation of a continuous cleft for substrate binding.⁴⁹

Despite the differences in loop flexibility of the key active site loops, two of which carry residues from the catalytic triad (Figure 1), we observe only subtle differences in the hydrogen-bonding patterns between the side chains of the catalytic serine (S160 in *IsPETase*) and histidine (H237 in *IsPETase*) and of the histidine and aspartate (D206 in *IsPETase*) for the *IsPETase*-based S214/I218 and H214/F218 variants of each system (Figures 3 and S7). It is worth noting that while the differences within each system are small, there is a more marked effect when comparing between different enzymes, and in particular between the mesophilic *IsPETase* and *BurPL* and the thermophilic *TfCut* and *LCC* enzymes. Here, all mesophilic enzymes exhibit substantially lower occupancy of the key hydrogen-bonding interactions, and in particular the serine–histidine interaction (Figure 3A), than their thermophilic counterparts. This is consistent with the fact that the key active site loops in the mesophilic enzymes are overall more flexible than their thermophile counterparts (Figure 2), even after introducing the serine and isoleucine double substitution, and may account for the reduced catalytic activity of the mesophiles compared to their thermophilic counterparts.^{12–14,20}

Following from this, we also calculated the volume of the active site cleft in all enzymes using POVME 3.0.⁴⁷ The resulting averages and standard deviations are shown in Table 1. As can be seen from these data, with the exception of *BurPL*, the *IsPETase*-based H214/F218 and S214/I218 variants of each system have similar active site volumes and fluctuations. However, there is quite a spread in active site volume and flexibility (using standard deviation as a proxy measure for flexibility), with *BurPL* and *TfCut* having the most compact and least flexible clefts, and *LCC* having the largest and most flexible cleft. The average cleft volume depends on its shape,

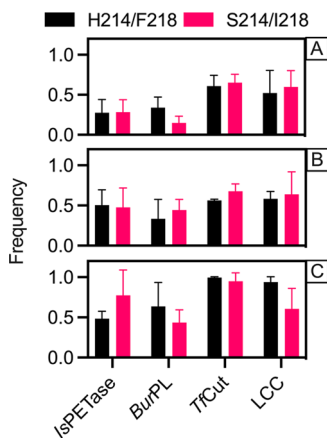


Figure 3. Frequency of interactions between key residues of the catalytic triad (Figure 1) during 5×500 ns simulations of each of the *IsPETase*-based S214/I218 and H214/F218 variants of PET hydrolases. Shown here are the relative frequencies of the interactions between (A) the hydroxyl group hydrogen of S160 and the N_e of H237, (B, C) the N_δ -bound hydrogen of H237 and each oxygen (B, $O_{\delta 1}$; C, $O_{\delta 2}$) from the carboxylic group of D206. The residue numbering corresponds to *IsPETase*. The error bars show the standard deviations across 5×500 ns conventional MD simulations of each system.

Table 1. Average Volumes of the Active Site Clefts of Each of *IsPETase*, *BurPL*, *TfCut*, and *LCC*, during Our Simulations^a

residues	open cleft volume (\AA^3)			
	<i>IsPETase</i>	<i>BurPL</i>	<i>TfCut</i>	<i>LCC</i>
H214/F218	187 ± 93	165 ± 44	189 ± 58	235 ± 98
S214/I218	192 ± 70	228 ± 59	188 ± 59	230 ± 102

^aAll values were calculated using POVM 3.0⁴⁷ and are presented as average values and standard deviations over 5×500 ns MD simulations per system, with snapshots taken every 2.5 ns of simulation time (2000 frames analyzed per system).

and on how many and how bulky the amino acid side chains which point inside the cleft are, whereas the volume fluctuations are intimately related to the structural flexibility of the cleft.

For all enzymes, the conserved W-loop tryptophan is facing a tyrosine residue, forming an aromatic clamp into which one of the terephthalic rings of PET binds.^{14,20} When W185 in *IsPETase* (PDB ID: 5XG0¹⁴) adopts conformer B, the distance between the C_γ atoms of this residue and Y87 in the aromatic clamp is 9.2 Å, whereas for conformer C, the distance is 7.8 Å (Figure S8). Therefore, we analyzed the change in distance between these aromatic residues in all MD simulations. As shown in Figure 4, a median distance of ~8.1 Å, similar to the experimental distance for the C conformer of W185, is obtained from the MD simulations for both *IsPETase* and *BurPL*. In contrast, a median distance of 8.9 Å, resembling the experimental distance for conformer B, is observed for simulations of *IsPETase* and *BurPL* with the S214/I218 substitutions. Finally, no differences are observed for the median distance of both variants of *TfCut* and *LCC*, with *TfCut* having a median distance 2 Å away from the crystallographic distance (PDB ID: 5ZOA³⁰), whereas *LCC* is closer to the experimental distance (PDB ID: 4EB0²⁷) (Figure S8).

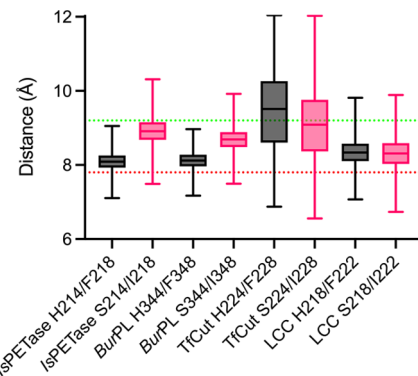


Figure 4. Box plot of the change in distance between the C_γ atom of the conserved tryptophan of the W-loop and the conserved tyrosine that completes the active site aromatic clamp, during 5×500 ns simulations of each of the *IsPETase*-based S214/I218 and H214/F218 PET hydrolase variants. The box length represents the interquartile range, which covers the central 50% of the data, and the horizontal line in the middle corresponds to the median, while the whiskers correspond to the minimum and maximum values. The dotted lines represent the experimental distances observed between Y87 and W185 in conformer B (red) and C (green) from *IsPETase* (PDB ID: 5XG0¹⁴).

Following from this, we performed shortest path map (SPM) analysis⁴⁸ on the MD replicas to analyze the allosteric communication pathways that potentially connect the different active site loop regions. The SPM method allows for the calculation of the shortest pathways between all residues (the nodes) in the network. Nodes and edges (pathways between nodes) that are often used for communication between residues can then be identified, and these residues can therefore be considered as being important for regulating the global conformational dynamics of the enzyme. The calculated allosteric communication pathways are presented in Figure 5 and illustrate the differences between enzymes from different source organisms. Loop D and the mutation-hosting helix are only mildly important for the pathway of both variants of *IsPETase*. In *BurPL*, loop H harbors significant residues whose motions are highly correlated. In *TfCut*, the network includes nodes on protein sections far from the active site.

When comparing the enzyme variants studied here, it is observed that the three loops, W, D, and H, appear linked to each other through different pathways on the identified networks. That is, with the exception of *IsPETase*, the SPM calculates a path connecting loops D and W in the cases of the histidine- and phenylalanine-containing variants (shown in red in Figure 5), whereas for *IsPETase*, this connection is absent in both H214/F218 and S214/I218 variants. For the H344/F348 variant of *BurPL*, the connection takes place between the W-loop tryptophan (W315) and the H344/F348 histidine. In *LCC* and *TfCut*, the correlation takes place between the tryptophan (W190 and W195 respectively) in loop W, and A213 and A219, respectively. It is therefore possible that both the enhanced fluctuations of loops H and D, and the decreased correlations of the dynamics of the conserved tryptophan in loop W with residues on loop D may depend on the bulkier nature of histidine and phenylalanine, which may exert additional steric repulsion on loop W.

Next, we explored the effect of the *IsPETase*-based serine and isoleucine double substitution on the conformational stability of the side chain of the conserved tryptophan from

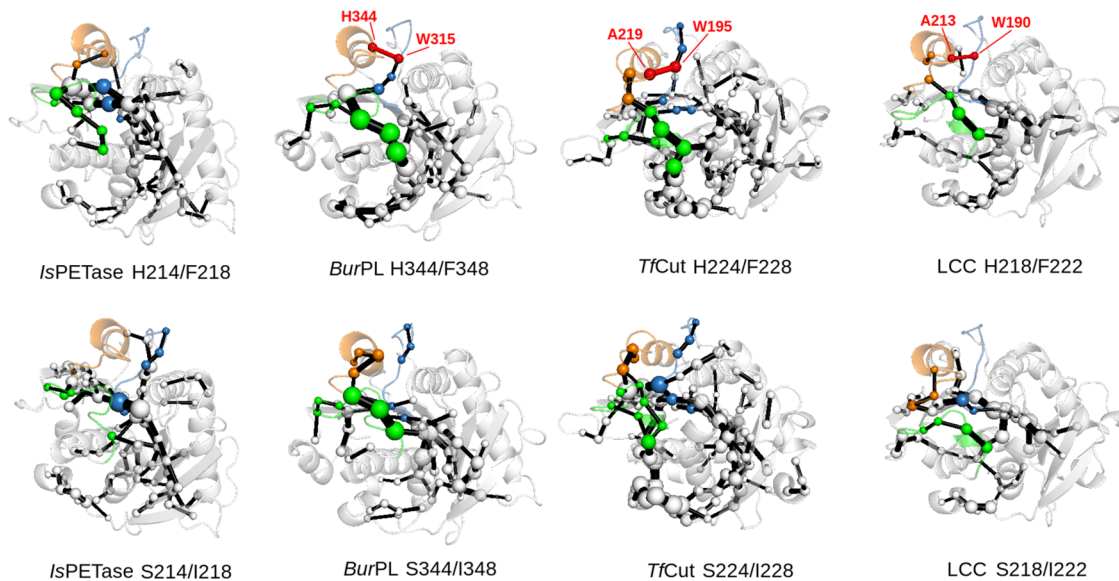


Figure 5. Representation of the shortest path map (SPM)⁴⁸ highlighting allosteric communication pathways in the different PET hydrolases studied in this work. The SPM is represented by spheres (residues) and edges (connections between residues), with the size of the spheres and edges being proportional to the number of pathways involving a sphere or edge, and a larger sphere size effectively meaning more importance of that residue for allosteric communication. Loop D and the S214/I218-H214/F218 containing helix are represented in orange, loop H in green, and loop W in blue. The path connecting loops W and D is shown in red (with residues involved labeled).

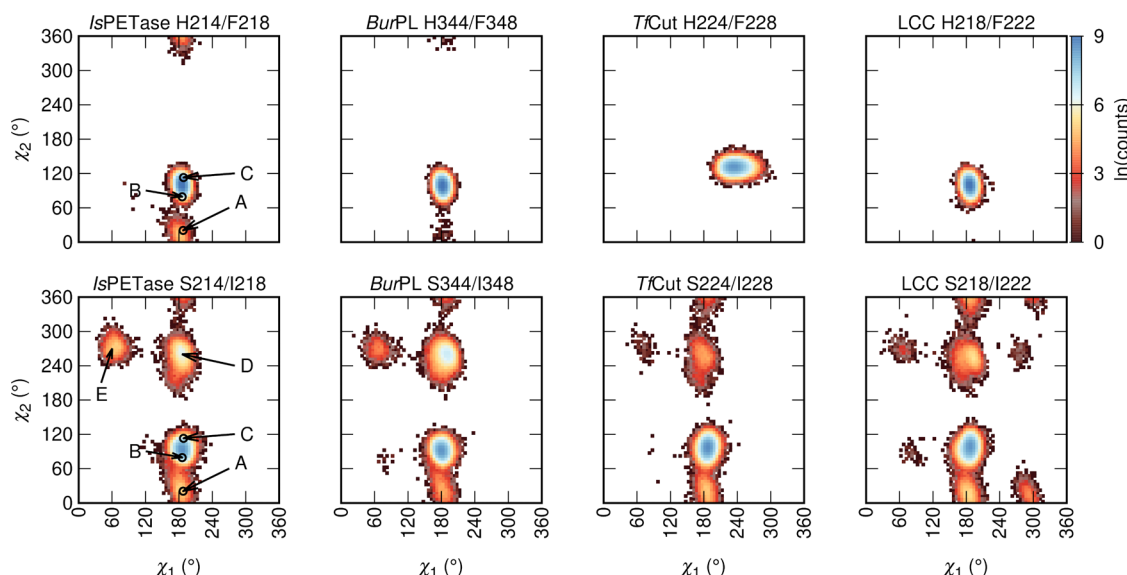


Figure 6. Torsional space explored by the W-loop tryptophan in the *IsPETase*-based H214/F218 and S214/I218 variants of PET hydrolases. The color gradient corresponds to the number of observations of a given χ_1 , χ_2 conformer in all MD trajectories for each system, cumulatively totaling 2.5 μ s simulation time per system (5×500 ns), with snapshots taken every 20 ps of simulation time. The arrows in *IsPETase* indicate the χ_1 , χ_2 torsion angles of the A, B, and C conformers observed in the crystal structures of *IsPETase*, and the new D and E conformers observed in our simulations.

loop W in our MD simulations. *IsPETase* residues S214 and I218, which correspond to histidine and phenylalanine in all other enzymes, are adjacent to W185 (Figure 1), with C_α – C_α distances to this residue of ~ 6 Å and ~ 9 Å, respectively, based on PDB ID: 5XG0.¹⁴ Crystal structures of *IsPETase* (PDB ID: 5XG0¹⁴) have shown that W185 can rotate into conformers A (chain A, $\chi_1 = 187.4^\circ$, $\chi_2 = 20.7^\circ$), B (chain B, $\chi_1 = 185.9^\circ$, $\chi_2 = 79.3^\circ$), and C (chain C, $\chi_1 = 188.2^\circ$, $\chi_2 = 113.1^\circ$).¹⁴ Upon binding of substrate analogues, W185 adopts conformer B^{14,15} (Figure 1).

To probe whether this plasticity is facilitated by the serine and isoleucine double substitution or by other features of the *IsPETase* scaffold, we calculated the χ_1 and χ_2 dihedral torsions of the corresponding tryptophan in all of the trajectories. From these data, it can be seen that the tryptophan side chain residue χ_1 and χ_2 dihedral angles are consistent with the B and C conformers of wild-type *IsPETase* in all of the H214/F218 and S214/I218 PET hydrolase variants (Figure 6). In contrast, the space created by the S214/I218 substitution and by the equivalent double substitution in *BurPL*, *TfCut*, and *LCC* enables the tryptophan to rotate into the A conformer in all

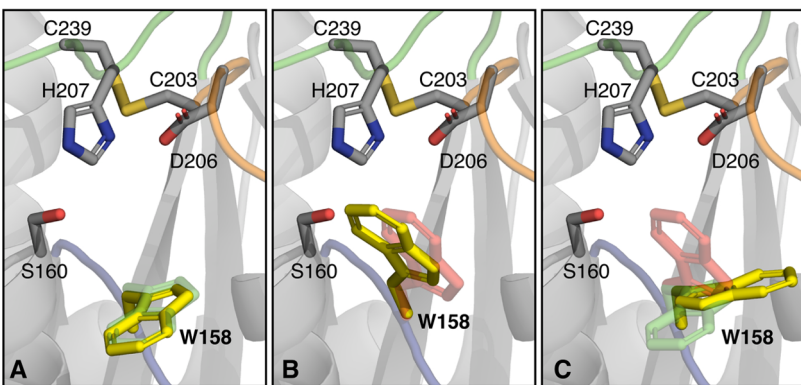


Figure 7. Representative structures of the different tryptophan conformations explored in our MD simulations. The residues of the catalytic triad and the W-loop tryptophan are shown in sticks, the MD-derived conformers for the W-loop tryptophan are shown in yellow, and the crystallographic conformers A and B are shown in red and green, respectively. (A, B) MD simulations exploring these conformers, whereas the conformer D from Figure 4, shown in (C), is only explored in the MD simulations and corresponds to a 180° rotation of the tryptophan side chain relative to conformer B.

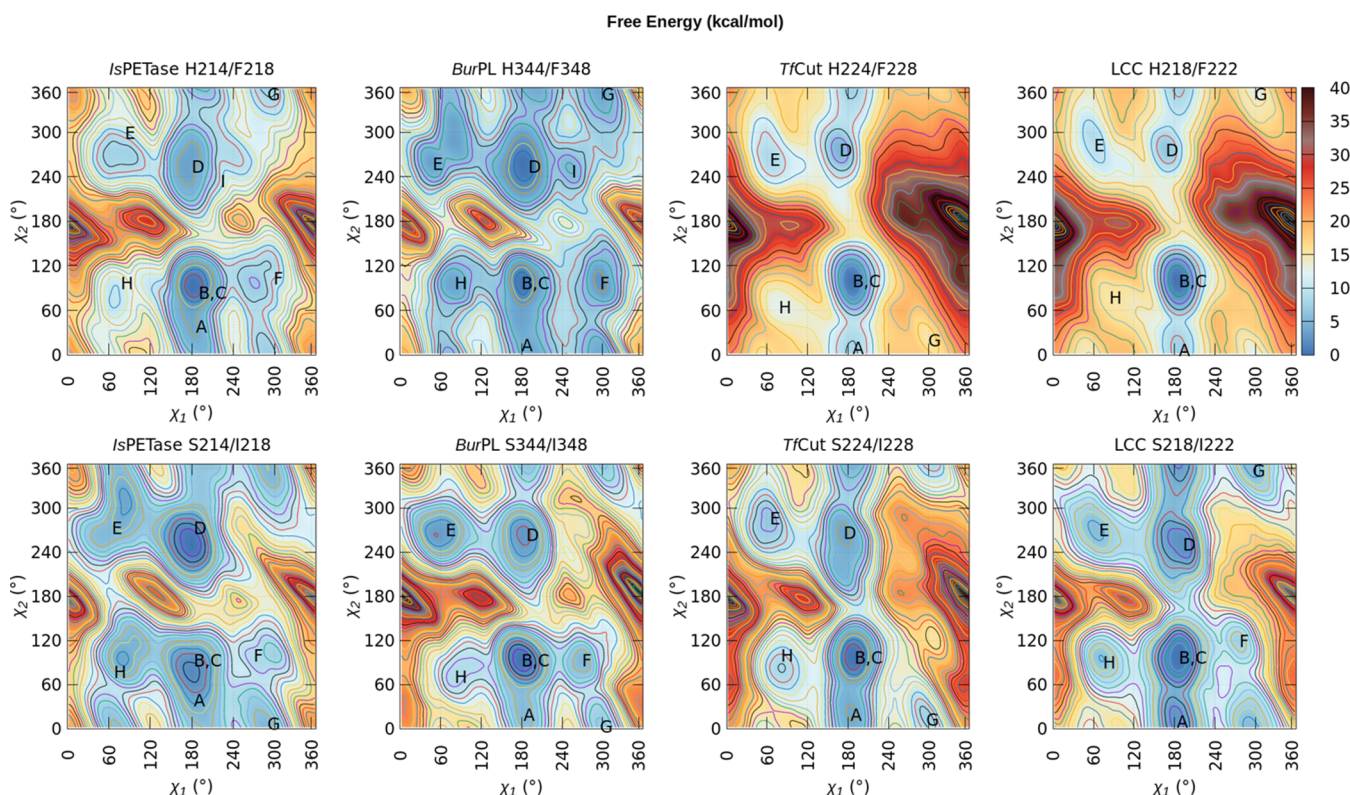


Figure 8. Free energy landscapes of the conformational space sampled by the side chain of the W-loop tryptophan in parallel-tempered metadynamics simulations of the *IsPETase*-based H214/F218 and S214/I218 variants of *IsPETase*, *BurPL*, LCC, and *TfCut*. Free energy landscapes were generated as a function of the χ_1 and χ_2 dihedral angles. The minimum free energy value is set to zero in every graph. The corresponding energy barriers are tabulated in Table S1.

PET hydrolases, as well as explore new conformations (Figures 6 and 7) that have not been captured in experimental structures. This is consistent with the expected plasticity of this residue in the unliganded form of the enzyme.¹⁴ This plasticity is lost in the H214/F218 variant of *IsPETase*, consistent with the observed loss of activity of the *IsPETase* S187H variant.¹⁴ These data highlight that the S214/I218 residues alone are sufficient to facilitate W185 and the equivalent residue in all other enzymes to rotate, without the need for other modifications to the scaffold, and that this “wobbling effect” appears to be transferable to other PET hydrolases.

Given the observed conformational plasticity of the conserved tryptophan residue in loop W, we opted to fully explore its torsional space via well-tempered metadynamics simulations,²⁸ in which the χ_1 and χ_2 dihedrals were used as collective variables (CVs). These simulations reached convergence within 400 ns, in terms of the diffusive behavior of the simulations (Figures S3 and S4). The free energy surfaces (FES) for each enzyme as a function of the two chosen CVs are presented in Figure 8. The overall landscape is conserved across all enzyme variants, with several common basins (labeled from A to I), separated by high energy barriers

(Figure 8 and Table S3). The D, E, and F basins correspond to the tryptophan side chain being oriented toward S/H214 and I/F218. In the F basin, the tryptophan is also proximal to the aspartic acid, in the I basin to the histidine and in the G basin to the serine of the catalytic triad, respectively. The H218/F222 variant of LCC and *TfCut* (either as H224/F228 or S224/I228) feature neither the F nor the I basins. The I basin is only present in the H214/F218 variant of *IsPETase* and H344/F348 variant of *BurPL*. For LCC and *TfCut*, the S218/I222 and S224/I228 mutations lower the barriers that connect the basins B, G, and E (Table S3). This is connected to an outward torsion of the tryptophan side chain (i.e., in the direction of the solvent), with the G basin corresponding to a conformation where the side chain shields the catalytic histidine from the solvent. The F basin in the S218/I222 mutant of LCC consists of the tryptophan side chain located in proximity to the catalytic residues.

Despite the overall topological similarities between the FES for each enzyme, important energetic differences are observed (Table S3). With the exception of *BurPL*, the different FES suggest that conformers A and B in the serine and isoleucine doubly substituted variants are nearly isoenergetic, in comparison to the energetic favorability of the B conformer in the histidine and phenylalanine variants. Since the neighboring side chains for these conformers are almost the same for all organisms, this probably arises from subtle dynamical effects of the W-loop. Specifically, for LCC and *TfCut*, this change in the energetics of the FES is accompanied by reductions of 4.4 and 3.3 kcal/mol in the relative free energy difference between the B and A basins, respectively (Table S3). These results suggest that the *IsPETase*-based S214/I218 substitutions result in enhanced “wobbling” of the W-loop tryptophan in these thermophilic enzymes, consistent with their 2- and 3-fold increase in activity against PET films.¹³ Similarly, conformer D is energetically more favorable for the *IsPETase*-based S214/I218 PETase variants in comparison to the histidine and phenylalanine variants in almost all cases, except for *BurPL*.

While our simulations are unable to elucidate the role of the new conformers observed by MD simulations for W185 in *IsPETase* and of the equivalent tryptophan residue in all variants of *BurPL*, *TfCut*, and LCC, recent works have provided valuable insights. Plastic degradation assays and MD simulations by Guo et al.⁵⁰ showed that PET polymers can bind in two different backbone conformations on the active site of *IsPETase*, *trans* (straight polymer conformation) and *gauche* (twisted polymer conformation), with a preferential selectivity for the *gauche* conformation that is abundant in PET films but absent in pretreated PET bottles. Interestingly, they design a *trans*-selective mutant (S238A) that has higher binding affinity to PET films than the wild-type enzyme and 3-fold higher activity against an all-*trans* PET substrate, which is enabled by W185 adopting conformer A to enable polymer binding in *trans*.⁵⁰

In addition, a similar work on computational and experimental engineering of *IsPETase* to enhance its activity against PET²² shows that W185 in the wild-type enzyme adopts conformers different from B to establish parallel displaced interactions with the terephthalic ring in the lowest-energy, catalytically competent predicted pose. Conversely, the W159H/S238F mutant, with higher activity against PET, binds the substrate in a conformer similar to B to establish T-shaped interactions. Moreover, when modeling the

binding of polyethylene-2,5-furandicarboxylate (PEF), an emerging bioplastic for replacing PET that is also degraded by *IsPETase*, W185 adopts conformers similar to D and A in the wild-type and W159H/S238F mutant enzymes, respectively.

CONCLUSIONS

In this work, we have performed a combination of MD and well-tempered metadynamics²⁸ simulations on four representative PET hydrolases with different optimal temperatures for hydrolytic activity, with the goal of providing an atomistic explanation on why the *IsPETase*-based S214/I218 substitution of two residues in the vicinity of the active site open cleft enhances the activity. Our investigation provides useful information regarding both the local dynamics of their active site. In particular, we have focused our attention on the flexibility of the active site and on the conformational plasticity of the side chain of a particularly important and highly conserved W-loop tryptophan, whose roles in the activity of these hydrolases have been previously demonstrated.^{14,20}

Our MD simulations illustrate that the S214/I218 substitution results in enhanced flexibility of the active site loops (as demonstrated by their higher fluctuations), in particular loop D that is connected to the helix that harbors the substituted residues. In turn, this flexibility allows the W-loop tryptophan and the tyrosine residue with which it forms an active site aromatic clamp²⁰ to occupy distances compatible with conformers for substrate binding in the two mesophilic enzymes studied. Even though the volume of the active site and its fluctuations over time are essentially unaltered by the mutations, we can speculate that the shape of the external part of the open cleft is, in the case of the *IsPETase*-based S214/I218 variants, amenable to accommodate the binding of a PET chain in the early stages of the overall degradation process. Validating this requires simulations that include the substrate docked into the binding pocket; whether this flexibility does in fact help substrate binding or product release will be a very interesting topic for future modeling studies. It is also clear that at the level of the global scaffold, the communication pathways differ by both organism and variant, which affects the flexibility of key loops and in turn the conformational sampling of the conserved tryptophan.

Regarding the conserved tryptophan, the unbiased MD simulations visited additional conformers A, D, and E for the *IsPETase*-based S214/I218 variants of PET hydrolases on a 500 ns timescale. Meanwhile, the free energy surfaces emerging from thorough exploration via metadynamics show how rotating through different basins is more likely in these PET hydrolase variants (which is true in general but it is particularly important for basins A and B), after elimination of the steric effects caused by the conserved histidine and phenylalanine residues.^{14,15} This enhanced rotation could be important for facilitating substrate binding and product release.

Prior work has proposed that these rotations of the conserved tryptophan are required to provide optimal aromatic interactions for the stabilization of substrate binding.²² Our insights complement these observations, suggesting that easy access and switch between different conformers of the conserved tryptophan is required for productive binding of different substrate conformations and possibly for product release to enable continued hydrolysis. The latter requires PET hydrolysis experiments in the presence of degradation products and simulations of enzyme–product complexes addressing the

molecular mechanisms of exiting the active site of PET hydrolases.

Evolutionary conformational selection is not unique to PET hydrolases: *de novo* designed Kemp eliminases such as the HG3⁵¹ and KE07^{52,53} series also possess conformational flexible and catalytically important tryptophan side chains in their active sites, the conformations of which are optimized during directed evolution. Similarly, laboratory evolution of an organophosphate hydrolase, serum paraoxonase 1, showed similar conformational effects in key active site residues along the evolutionary trajectory.⁵⁴ Similarly to these systems, our results suggest that engineering of PET hydrolases with mutations that enable conformational selection of the conserved tryptophan, such as S214/I218 and the S238A mutation in *IsPETase*, could lead to predefined active site conformations matching the polymer conformations in PET materials and enable higher catalytic efficiency. Further computational and experimental work is necessary to explore how different tryptophan conformations enable higher catalytic activity in natural and engineered PET hydrolases.

■ ASSOCIATED CONTENT

Data Availability Statement

The data underlying this study are available in the published article and its online supplementary material. A companion data package including input files, starting structures, and simulation snapshots has been submitted to Zenodo at the following DOI: 10.5281/zenodo.7158149.

■ Supporting Information

The Supporting Information is available free of charge at <https://pubs.acs.org/doi/10.1021/acsorginorgau.2c00054>.

RMSD of production runs for molecular dynamics and equilibration runs for metadynamics simulations; diffusive behavior of the metadynamics simulations; additional structural analysis; and free energy differences between the different conformational states ([PDF](#))

■ AUTHOR INFORMATION

Corresponding Authors

Shina C. L. Kamerlin — Department of Chemistry—BMC, Uppsala University, S-751 23 Uppsala, Sweden; School of Chemistry and Biochemistry, Georgia Institute of Technology, Atlanta, Georgia 30332-0400, United States;  [orcid.org/0000-0002-3190-1173](#); Email: skamerlin3@gatech.edu

César A. Ramírez-Sarmiento — Institute for Biological and Medical Engineering, Schools of Engineering, Medicine and Biological Sciences, Pontificia Universidad Católica de Chile, Santiago 7820436, Chile; ANID—Millennium Science Initiative Program—Millennium Institute for Integrative Biology (*iBio*), Santiago 8331150, Chile;  [orcid.org/0000-0003-4647-903X](#); Email: cesar.ramirez@uc.cl

Authors

Alessandro Crnjar — Department of Chemistry—BMC, Uppsala University, S-751 23 Uppsala, Sweden

Aransa Griñen — Institute for Biological and Medical Engineering, Schools of Engineering, Medicine and Biological Sciences, Pontificia Universidad Católica de Chile, Santiago 7820436, Chile; ANID—Millennium Science Initiative Program—Millennium Institute for Integrative Biology (*iBio*), Santiago 8331150, Chile

Complete contact information is available at:
<https://pubs.acs.org/10.1021/acsorginorgau.2c00054>

Author Contributions

¹A.C. and A.G. contributed equally to this work. CRediT: Alessandro Crnjar conceptualization (equal), data curation (equal), formal analysis (equal), investigation (equal), methodology (equal), writing-original draft (equal), writing-review & editing (equal); Aransa Griñen formal analysis (equal), investigation (equal), writing-original draft (equal), writing-review & editing (equal); Shina C. L. Kamerlin conceptualization (equal), data curation (equal), formal analysis (equal), funding acquisition (equal), investigation (equal), methodology (equal), project administration (equal), resources (equal), software (equal), supervision (equal), validation (equal), writing-original draft (equal), writing-review & editing (equal); Cesar A. Ramírez-Sarmiento conceptualization (equal), data curation (equal), formal analysis (equal), funding acquisition (equal), investigation (equal), methodology (equal), project administration (equal), resources (equal), software (equal), supervision (equal), validation (equal), visualization (equal), writing-original draft (equal), writing-review & editing (equal).

Notes

The authors declare no competing financial interest.

■ ACKNOWLEDGMENTS

This research was funded by the National Agency for Research and Development (ANID) and the São Paulo Research Foundation (grant ANID-FAPESP 2019/13259-9), the ANID Millennium Science Initiative Program (grant ICN17_022), and the Knut and Alice Wallenberg Foundation (grant nos. 2018.0140 and 2019.0431). Aransa Griñen was supported by an ANID doctoral scholarship (PFCHA 21220450). Powered@NLHPC: This research was partially supported by the supercomputing infrastructure of the NLHPC (ECM-02). Further simulations were enabled by resources provided by the Swedish National Infrastructure for Supercomputing (SNIC: SNIC2020-3-1 and SNIC2021-3-1), partially funded by the Swedish Research Council [Grant 2016-07213].

■ REFERENCES

- (1) Geyer, R.; Jambeck, J. R.; Lavender Law, K. Production, Use, and Fate of All Plastics Ever Made. *Sci. Adv.* **2017**, *3*, No. e1700782.
- (2) Schyns, Z. O. G.; Shaver, M. P. Mechanical Recycling of Packaging Plastics: A Review. *Marcomol. Rapid Commun.* **2021**, *42*, No. e2000415.
- (3) La Mantia, F. P.; Vinci, M. Recycling Poly(ethylene terephthalate). *Polym. Degrad. Stab.* **1994**, *45*, 121–125.
- (4) Hong, M.; Chen, E. Y.-X. Chemically Recyclable Polymers: A Circular Economy Approach to Sustainability. *Green Chem.* **2017**, *19*, 3692–3706.
- (5) Kawai, F.; Kawabata, T.; Oda, M. Current Knowledge on Enzymatic PET degradation and its Possible Application to Waste Stream Management and Other Fields. *Appl. Microbiol. Biotechnol.* **2019**, *103*, 4253–4268.
- (6) Taniguchi, I.; Yoshida, S.; Hiraga, K.; Miyamoto, K.; Kimura, Y.; Oda, K. Biodegradation of PET: Current Status and Application Aspects. *ACS Catal.* **2019**, *9*, 4089–4105.
- (7) Salvador, M.; Abdulmutalib, U.; Gonzalez, J.; Kim, J.; Smith, A. A.; Faulon, J.-L.; Wei, R.; Zimmermann, W.; Jimenez, J. I. Microbial Genes for a Circular and Sustainable Bio-PET Economy. *Genes* **2019**, *10*, 373.

- (8) Wei, R.; Zimmermann, W. Microbial Enzymes for the Recycling of Recalcitrant Petroleum-Based Plastics: How Far Are We? *Microb. Biotechnol.* **2017**, *10*, 1308–1322.
- (9) Sonnendecker, C.; Oeser, J.; Richter, P. K.; Hille, P.; Zhao, Z.; Fischer, C.; Lippold, H.; Blázquez-Sánchez, P.; Engelberger, F.; Ramírez-Sarmiento, C. A.; Oeser, T.; Lihanova, Y.; frank, R.; Jahnke, H.-G.; Billig, S.; Abel, B.; Sträter, N.; Matysik, J.; Zimmermann, W. Low Carbon Footprint Recyclinc of Post-Consumer PET Plastic with a Metagenomic Polyester Hydrolase. *ChemSusChem* **2022**, *15*, No. e202101062.
- (10) Thomsen, T. B.; Hunt, C. J.; Meyer, A. S. Influence of Substrate Crystallinity and Glass Transition Temperature on Enzymatic Degradation of Polyethylene Terephthalate (PET). *New Biotechnol.* **2022**, *69*, 28–35.
- (11) Yoshida, S.; Hiraga, K.; Takahena, T.; Taniguchi, I.; Yamaji, H.; Maeda, Y.; Toyohara, K.; Miyamoto, K.; Kimura, Y.; Oda, K. A Bacterium That Degrades and Assimilates Poly(ethylene terephthalate). *Science* **2016**, *351*, 1196–1199.
- (12) Wei, R.; von Haugwitz, G.; Pfaff, L.; Mican, J.; Badenhorst, C. P. S.; Liu, W.; Weber, G.; Austin, H. P.; Bednar, D.; Damborsky, J.; Bornscheuer, U. T. Mechanism-Based Design of Efficient PET Hydrolases. *ACS Catal.* **2022**, *12*, 3382–3396.
- (13) Chen, C.-C.; Han, X.; Li, X.; Jiang, P.; Niu, D.; Ma, L.; W, L.; Li, S.; Qu, Y.; Hu, H.; Min, J.; Yang, Y.; Zhang, L.; Zeng, W.; Huang, J.-W.; Dai, L.; Guo, R.-T. General Features to Enhance Enzymatic Activity of Poly(ethylene Terephthalate) Hydrolysis. *Nat. Catal.* **2021**, *4*, 425–430.
- (14) Han, X.; Liu, W.; Huang, J.-W.; Ma, J.; Zheng, Y.; Ko, T.-P.; Xu, L.; Cheng, Y.-S.; Chen, C.-C.; Guo, R.-T. Structural Insight into Catalytic Mechanism of PET Hydrolase. *Nat. Commun.* **2017**, *8*, No. 2106.
- (15) Chen, C.-C.; Han, X.; Ko, T.-P.; Liu, W.; Guo, R.-T. Structural Studies Reveal the Molecular Mechanism of PETase. *FEBS J.* **2018**, *285*, 3717–3723.
- (16) Jerves, C.; Neves, R. P. P.; Ramos, M. J.; da Silva, S.; Fernandes, P. A. Reaction Mechanism of the PET Degrading Enzyme PETase Studied with DFT/MM Molecular Dynamics Simulations. *ACS Catal.* **2021**, *11*, 11626–11638.
- (17) Pinto, A. V.; Ferreira, P.; Neves, R. P. P.; Fernandes, P. A.; Ramos, M. J.; Magalhães, A. L. Reaction Mechanism of MHETase, a PET Degrading Enzyme. *ACS Catal.* **2021**, *11*, 10416–10428.
- (18) Boneta, S.; Arafet, K.; Moliner, V. QM/MM Study of the Enzymatic Biodegradation Mechanism of Polyethylene Terephthalate. *J. Chem. Inf. Model.* **2021**, *61*, 3041–3051.
- (19) Magalhães, R. P.; Fernandes, H. S.; Sousa, S. F. The Critical Role of Asp206 Stabilizing Residues on the Catalytic Mechanism of the *Ideonella sakaiensis* PETase. *Catal. Sci. Technol.* **2022**, *12*, 3474–3483.
- (20) Fecker, T.; Galaz-Davison, P.; Engelberger, F.; Narui, Y.; Sotomayor, M.; Parra, L. P.; Ramírez-Sarmiento, C. A. Active Site Flexibility as a Hallmark for Efficient PET Degradation by *I. sakaiensis* PETase. *Biophys. J.* **2018**, *114*, 1302–1312.
- (21) da Costa, C. H. S.; Santos, Dos.; Alves, A. M.; Martí, C. N.; Moliner, S.; Santana, V.; Lameira, K.; Assessment, J. of the PETase Conformational Changes Induced by Poly(Ethylene Teraphthalate) Binding. *Proteins: Struct., Funct., Bioinf.* **2021**, *89*, 1340–1352.
- (22) Austin, H. P.; Allen, M. D.; Donohoe, B. S.; Rorrer, N. A.; Kean, F. L.; Silveira, R. L.; Pollard, B. C.; Dominick, G.; Duman, R.; El Omari, K.; Mykhaylyk, V.; Wagner, A.; Michener, W. E.; Amore, A.; Skaf, M. S.; Crowley, M. F.; Thorne, A. W.; Johnson, C. W.; Woodcock, H. L.; McGeehan, J. E.; Beckham, G. T. Characterization and Engineering of a Plastic-Degrading Aromatic Polyesterase. *Proc. Natl. Acad. Sci. U.S.A.* **2018**, *115*, E4350–E4357.
- (23) Knott, B. C.; Erickson, E.; Allen, M. D.; Gado, J. E.; Graham, R.; Kearns, F. L.; Pardo, I.; Topuzlu, E.; Anderson, J. J.; Austin, H. P.; Dominick, G.; Johnson, C. W.; Rorrer, N. A.; Skostkiewicz, C. J.; Copié, V.; Payne, C. M.; Woodcock, H. L.; Donohoe, B. S.; Beckham, G. T.; McGeehan, J. E. Characterization and Engineering of a Two-Enzyme System for Plastics Depolymerization. *Proc. Natl. Acad. Sci. U.S.A.* **2020**, *117*, 25476–25485.
- (24) Lu, H.; Diaz, D. J.; Czarnecki, N. J.; Zhu, C.; Kim, W.; Shroff, R.; Acosta, D. J.; Alexander, B. R.; Cole, H. O.; Zhang, Y.; Lynd, N. A.; Ellington, A. D.; Alper, H. S. Machine Learning-Aided Engineering of Hydrolases for PET Depolymerization. *Nature* **2022**, *604*, 662–667.
- (25) Joho, Y.; Vongsouthi, V.; Spence, M. A.; Ton, J.; Gomez, C.; Tan, L. L.; KaczmarSKI, J. A.; Caputo, A. T.; Royan, S.; Jackson, C. J.; Ardevol, A. Ancestral Sequence Reconstruction Identifies Structural Changes Underlying the Evolution of *Ideonella sakaiensis* PETase and Variants with Improved Stability and Activity. *Biochemistry* **2022**, DOI: 10.1021/acs.biochem.2c00323.
- (26) Müller, R.-J.; Schrader, H.; Profe, J.; Dresler, K.; Deckwer, W.-D. Enzymatic Degradation of Poly(ethylene Terephthalate): Rapid Hydrolysis Using a Hydrolase from *T. fusca*. *Macromol. Rapid Commun.* **2005**, *26*, 1400–1405.
- (27) Sulaiman, S.; Yamato, S.; Kanaya, E.; Kim, J.-J.; Koga, Y.; Takano, K.; Kanaya, S. Isolation of a Novel Cutinase Homolog with Polyethylene Terephthalate-Degrading Activity from Leaf-Branch Compost Using a Metagenomic Approach. *Appl. Environ. Microbiol.* **2012**, *78*, 1556–1562.
- (28) Barducci, A.; Bussi, G.; Parrinello, M. Well-Tempered Metadynamics: A Smoothly Converging and Tunable Free-Energy Method. *Phys. Rev. Lett.* **2008**, *100*, No. 020603.
- (29) Berman, H. M.; Westbrook, J.; Feng, Z.; Gilliland, G.; Bhat, T. N.; Weissig, H.; Shindyalov, I. N.; Bourne, P. E. The Protein Data Bank. *Nucleic Acids Res.* **2000**, *28*, 235–242.
- (30) Dong, Q.; Yuan, S.; Wu, L.; Su, L.; Zhao, Q.; Wu, J.; Huang, W.; Zhuo, J. Structure-Guided Engineering of a *Thermobifida fusca* Cutinase for Enhanced Hydrolysis on Natural Polyester Substrate. *Bioresour. Bioprocess.* **2020**, *7*, No. 37.
- (31) The PyMOL Molecular Graphics System; Schrödinger, LLC.
- (32) The Uniprot Consortium. UniProt: The Universal Protein Knowledgebase. *Nucleic Acids Res.* **2018**, *46*, 2699.
- (33) Case, D. A.; Belfon, K.; Ben-Shalom, I. Y.; Brozell, S. R.; Cerutti, D. S.; Cheatham, T. E., III; Cruzeiro, V. W. D.; Darden, T. A.; Duke, R. E.; Giambasu, G.; Gilson, M. K.; Gohlke, H.; Goetz, A. W.; Harris, R.; Izadi, S.; Izmailov, S. A.; Kasavajhala, K.; Kovalenko, A.; Krasny, R.; Kurtzman, T.; Lee, T. S.; LeGrand, S.; Li, P.; Lin, C.; Liu, J.; Luchko, T.; Luo, R.; Man, V.; Merz, K. M.; Miao, Y.; Mikhailovskii, O.; Monard, G.; Nguyen, H.; Onufriev, A.; Pan, F.; Pantano, S.; Qi, R.; Roe, D. R.; Roitberg, A.; Sagui, C.; Schott-Verdugo, S.; Shen, J.; Simmerling, C. L.; Skrynnikov, N. R.; Smith, J.; Swails, J.; Walker, R. C.; Wang, J.; Wilson, L.; Wolf, R. M.; Wu, X.; Xiong, Y.; Xue, Y.; York, D. M.; Kollman, P. A. AMBER 2020; University of California: San Francisco, 2020.
- (34) Maier, J. A.; Martinez, C.; Kasavajhala, K.; Wickstrom, L.; Hauser, K. E.; Simmerling, C. FF14SB: Improving the Accuracy of Protein Side Chain and Backbone Parameters from FF99SB. *J. Chem. Theory. Comput.* **2015**, *11*, 3696–3713.
- (35) Jorgensen, W. L.; Chandrasekhar, J.; Madura, J. D.; Impey, R. W.; Klein, M. L. Comparison of Simple Potential Functions for Simulating Liquid Water. *J. Chem. Phys.* **1983**, *79*, 926–935.
- (36) Anandakrishnan, R.; Aguilar, B.; Onufriev, A. V. H++ 3.0: Atomistic pK Prediction and the Preparation of Biomolecular Structures for Atomistic Molecular Modeling and Simulations. *Nucleic Acids Res.* **2012**, *40*, W537–W541.
- (37) Pastor, R. W.; Brooks, B. R.; Szabo, A. An Analysis of the Accuracy of Langevin and Molecular Dynamics Algorithms. *Mol. Phys.* **1988**, *65*, 1409–1419.
- (38) Berendsen, H. J. C.; Postma, J. P. M.; van Gunsteren, W. F.; DiNola, A.; Haak, J. R. Molecular Dynamics with Coupling to an External Bath. *J. Chem. Phys.* **1984**, *81*, 3684–3690.
- (39) Ryckaert, J.-P.; Ciccotti, G.; Berendsen, H. J. C. Numerical Integration of the Cartesian Equations of Motion of a System with Constraints: Molecular Dynamics of n-Alkanes. *J. Comput. Phys.* **1977**, *23*, 327–341.

- (40) Darden, T.; York, D.; Pedersen, L. Particle Mesh Ewald: An $N \log(N)$ Method for Ewald Sums in Large Systems. *J. Chem. Phys.* **1993**, *98*, 10089–10092.
- (41) Tribello, G. A.; Bonomi, M.; Branduardi, D.; Camilloni, C.; Bussi, G. PLUMED 2: New Feathers for an Old Bird. *Comput. Phys. Commun.* **2014**, *185*, 604–613.
- (42) Laio, A.; Parrinello, M. Escaping Free Energy Minima. *Proc. Natl. Acad. Sci. U.S.A.* **2002**, *99*, 12562–12566.
- (43) Tiwary, P.; Parrinello, M. A.; Time-Independent, A. Free Energy Estimator for Metadynamics. *J. Phys. Chem. B* **2015**, *119*, 736–742.
- (44) Roe, D. R.; Cheatham, T. E. PTRAJ and CPPTRAJ: Software for Processing and Analysis of Molecular Dynamics Trajectory Data. *J. Chem. Theory Comput.* **2013**, *9*, 3084–3095.
- (45) Michaud-Agrawal, N.; Denning, E. J.; Woolf, T. B.; Beckstein, O. MDAnalysis: A Tool for the Analysis of Molecular Dynamics Simulations. *J. Comput. Chem.* **2011**, *32*, 2319–2327.
- (46) Gowers, R.; Linke, M.; Barnoud, J.; Reddy, T.; Melo, M.; Seyler, S.; Domanski, J.; Dotson, D.; Buchoux, S.; Kenney, I.; Beckstein, O. In *MDAnalysis: A Python Package for the Rapid Analysis of Molecular Dynamics Simulations*, Proceedings of the 15th Python in Science Conference, 2016.
- (47) Wagner, J. R.; Sørensen, J.; Hensley, N.; Wong, C.; Zhu, C.; Perison, T.; Amaro, R. E. POVME 3.0: Software for Mapping Binding Pocket Flexibility. *J. Chem. Theory Comput.* **2017**, *13*, 4584–4592.
- (48) Romero-Rivera, A.; Garcia-Borras, M.; Osuna, S. Role of Conformational Dynamics in the Evolution of Retro-Aldolase Activity. *ACS Catal.* **2017**, *7*, 8524–8532.
- (49) Joo, S.; Cho, I. J.; Seo, H.; Son, H. F.; Sagong, H.-Y.; Shin, T. J.; Choi, S. Y.; Lee, S. Y.; Kim, K.-J. Structural Insight Into Molecular Mechanism of Poly(Ethylene Terephthalate) Degradation. *Nat. Commun.* **2018**, *9*, No. 382.
- (50) Guo, B.; Vanga, S. R.; Lopez-Loreno, X.; Saenz-Mendez, P.; Ericsson, S. R.; Fang, Y.; Ye, X.; Schriever, K.; Bäckström, E.; Biundo, A.; Zubarev, R. A.; Furó, I.; Hakkarainen, M.; Syrén, P.-O. Conformational Selection in Biocatalytic Plastic Degradation by PETase. *ACS Catal.* **2022**, *12*, 3397–3409.
- (51) Blomberg, R.; Kries, H.; Pinkas, D. M.; Mittl, P. R. E.; Grütter, M. G.; Privett, H. K.; Mayo, S. L.; Hilvert, D. Precision is Essential for Efficient Catalysis in an Evolved Kemp Eliminase. *Nature* **2013**, *503*, 418–421.
- (52) Röthlisberger, D.; Khersonsky, O.; Wollacott, A. W.; Jiang, L.; DeChancie, J.; Betker, J.; Gallaher, J. L.; Althoff, E. A.; Zanghellini, A.; Dym, O.; Albeck, S.; Houk, K. N.; Tawfik, D. S.; Baker, D. Kemp Elimination Catalysts by Computational Enzyme Design. *Nature* **2008**, *453*, 190–195.
- (53) Hong, N.-S.; Petrovic, D.; Lee, R.; Gryn'ova, G.; Purg, M.; Saunders, J.; Bauer, P.; Carr, P. D.; Lin, C.-Y.; Mabbitt, P. D.; Zhang, W.; Altamore, T.; Easton, C.; Coote, M. L.; Kamerlin, S. C. L.; Jackson, C. J. The Evolution of Multiple Active Site Configurations in a Designed Enzyme. *Nat. Commun.* **2018**, *9*, No. 3900.
- (54) Ben-David, M.; Soskine, M.; Dubovetskyi, A.; Cherukuri, K.-P.; Dym, O.; Sussman, J. L.; Liao, Q.; Szeler, K.; Kamerlin, S. C. L.; Tawfik, D. S. Enzyme Evolution: An Epistatic Ratchet versus a Smooth Reversible Transition. *Mol. Biol. Evol.* **2020**, *37*, 1133–1147.